

Phase transition dynamics for baryon-dense matter

Jørgen Randrup

Nuclear Science Division, Lawrence Berkeley National Laboratory, Berkeley, California 94720, USA

(Dated: March 27, 2009)

We construct a simple two-phase equation of state intended to resemble that of compressed baryon-rich matter and then introduce a gradient term in the compressional energy density to take account of finite-range effects in non-uniform configurations. With this model we study the interface between the two coexisting phases and obtain estimates for the associated interface tension. Subsequently, we incorporate the finite-range equation of state into ideal or viscous fluid dynamics and derive the collective dispersion relation for the mechanically unstable modes of bulk matter in the spinodal region of the thermodynamic phase diagram. Combining these results with time scales extracted from existing dynamical transport simulations, we discuss the prospects for spinodal phase separation to occur in nuclear collisions. We argue that these can be optimized by a careful tuning of the collision energy to maximize the time spent by the bulk of the system inside the mechanically unstable spinodal region of the phase diagram. Our specific numerical estimates suggest cautious optimism that this phenomenon may in fact occur, though a full dynamical simulation is needed for a detailed assessment.

PACS numbers: 25.75.-q, 81.30.Dz, 64.75.Gh, 64.60.an

I. INTRODUCTION

The phase structure of strongly interacting matter presents a focal point for current theoretical and experimental investigations. In particular, the Relativistic Heavy Ion Collider (RHIC) at BNL is preparing for a beam energy scan that aims to identify signals of the expected critical point and the CBM experiment at the future Facility for Antiproton and Ion Research (FAIR) at GSI will explore the properties of compressed baryonic matter and search for the expected first-order phase transition.

On the theoretical side, the situation is far from clear. Whereas lattice QCD calculations [1, 2] find that the deconfinement phase transformation is of the crossover type at vanishing chemical potential, $\mu = 0$, they have inherent difficulties treating finite μ values and any predictions in the baryon-rich domain are still very uncertain [3, 4, 5]. Even the very existence of a critical point has recently been called into doubt [6]. Experimental information would therefore be invaluable.

However, it will be no easy task to extract the thermodynamic phase structure from nuclear collision experiments. In addition to the inherent problems arising from the smallness of the collision system (which renders its spatial configuration far from uniform) and its rapid evolution (which prevents global equilibrium from being established), the experimentalist is faced with the problem that there exists yet no suitable dynamical model with which to simulate the collisions for the purpose of anticipating the observable effects of the phase structure.

This crucial point deserves elaboration: First of all, the basic theory, quantum chromodynamics, is currently tractable only in either the perturbative limit of hard elementary processes or in the thermodynamic limit at vanishing (or small) net baryon density. Any dynamical

transport treatment of nuclear collisions must therefore involve a considerable degree of modeling.

Ideally, one would devise a transport model that explicitly treats the dynamics of the microscopic degrees of freedom in the system, which change from being partonic in the deconfined sector to being hadronic in the confined sector. Unfortunately, it has yet not been possible to develop such a description, even for static scenarios. Nevertheless, a variety of microscopic transport models have achieved considerable success with regard to calculating (and reproducing) observables for high-energy collisions over a large range of energies. However, their thermodynamic properties are (yet) inadequate. For one thing, they usually lack detailed balance (as is often well justified in the context of the dynamical processes for which they are intended) and therefore they are inadequate for thermal equilibrium. Furthermore, these models do not (as of yet) incorporate a first-order phase transition. Therefore, at this point, they appear to be unsuitable for simulations that aim to bring out the dynamical effects of a phase transition and elucidate their observability.

Considerable success has been obtained as well with macroscopic models within the framework of fluid dynamics. These models have the practical advantage that the underlying microscopic degrees of freedom do not enter explicitly, the state of the system being described merely through its local energy and charge densities (and the associated currents) with the interactions entering via the equation of state and the transport coefficients. [Of course, in order to make contact with experiment, such a treatment must ultimately convert the macroscopic information into hadrons by a suitable freeze-out prescription, but this occurs at densities well below the phase transition region and is well developed.] Thus fluid dynamics, especially ideal fluid dynamics for which the transport coefficients vanish, possesses a very close relationship be-

tween the dynamics and the underlying object of study, the equation of state.

However, a closer analysis reveals that standard fluid dynamics has certain inherent problems in the presence of a first-order phase transition. Of particular importance is the fact that standard fluid dynamics is strictly local which leads to both static and dynamic shortcomings, as we shall now discuss.

With regard to the former, imagine that two thermodynamically coexisting bulk systems are brought into contact along a common interface. In a realistic description, a diffuse interface would develop, with the various densities changing smoothly from one bulk value to the other, and there would be an interface tension. By contrast, when the equation of state is strictly local, the interface will be sharp (so the various densities will change abruptly from one bulk value to the other across the interface) and there will be no interface tension. Such a description would not be adequate for finite systems such as blobs of matter produced in a collision, whose sizes are determined primarily by the surface tension and for which much of the matter is located in the diffuse surface region. While this generic shortcoming may be less serious for high-energy collisions, where the matter is being torn apart due to the rapid longitudinal stretching, it is expected to play a significant role at the lower collision energies relevant for the exploration of the deconfinement phase transition.

As for the dynamics, consider the evolution of nearly uniform matter that has been prepared in a state of expansion at a density just above the phase coexistence region. The system would then continue its expansion and the associated phase point would soon enter the phase coexistence region in which uniform matter is thermodynamically metastable. While this would pose no particular problem as long as the deviations from uniformity remain small, the further expansion would drive the phase point into the region of spinodal instability, where uniform matter is both thermodynamically and mechanically unstable (the speed of sound is imaginary). As a result, density undulations would (and should) become amplified.

This scenario is familiar from many areas of physics and it has been studied both theoretically and experimentally for a variety of substances [7, 8]. Generally, the associated collective dispersion relation (which in this situation gives the growth rate as a function of the wave number, γ_k) exhibits a maximum, thus leading to preferential amplification of certain modes and the appearance of a characteristic length scale in the ensuing phase separation. This remarkable phenomenon, known as spinodal phase decomposition, is an indicator of a first-order phase transition. It was found to present a powerful means for the experimental exploration of the nuclear liquid-gas phase transition [8, 9], because the unstable dilute bulk matter tends to condense into fragments of similar sizes, a highly non-statistical outcome that is easy to identify in the event analysis. This success has given rise

to the hope that spinodal decomposition could be useful as well for probing the confinement phase transition and some explorations of possible experimental signals have already been made [10, 11, 12, 13].

Naturally, since standard fluid dynamics is local, so is its collective dispersion relation, $\omega_k = v_0 k$. Consequently, inside the spinodal region of the phase diagram, the growth rate will increase monotonically with the wave number of the undulation. Thus γ_k will not display a maximum and the characteristic spinodal decomposition phenomenon would not develop, as density irregularities of ever smaller scale would be amplified at ever larger rates. In ideal fluid dynamics, this problem would be computationally intractable (and in fact mathematically meaningless) [14]. The inclusion of viscosity would modulate the dispersion relation and cause the growth rate to approach a constant value for large k . While this would facilitate the numerics, the monotonic growth of γ_k would still preclude the occurrence of a spinodal decomposition.

Because of the considerable potential for fluid dynamics as a tool for obtaining insight into the phase transition dynamics, we address here this generic shortcoming. Our main purpose is to illustrate the advantages of remedying this problem and, along the way, make rough estimates for various key quantities. Since the problem arises from the local nature of fluid dynamics, we introduce a finite range into the treatment by means of a gradient term in the compressional energy density. The specific model developed here is intended to serve mainly as a framework for illustrating the effect of incorporating a finite range into the dynamical description and the specific quantitative results should be regarded as correspondingly rough.

We first (Sect. II) construct a somewhat schematic equation of state for uniform matter, trying to incorporate the most essential features expected; it should be considered as merely a temporary substitute subject to refinement. Subsequently (Sect. III) the finite range is introduced by means of a simple gradient term. Then (Sect. IV) we consider the equilibrium interface between two bulk systems, a property that could not be addressed with the standard treatment due to its strict locality, and obtain expressions for the associated interface tension. The collective modes in bulk matter are then treated (Sect. V) and we consider particularly the spinodal growth rates which now display the characteristic features known from other substances. Finally (Sect. VI), on this basis, we discuss the phase transition dynamics expected for the planned nuclear collision experiments and the prospects for spinodal decomposition to actually occur.

II. BULK MATTER EQUATION OF STATE

We wish to employ an equation of state that is suitable for numerical illustrations. For this purpose, we design a schematic model that is a generalization of a classical gas in a density-dependent mean field. The resulting

equation of state has certain generic deficiencies and the results should therefore not be taken at face value. [For example, there are no bosonic degrees of freedom.] It would of course be of interest to repeat the present analysis as more refined descriptions become available.

The equation of state provides the thermodynamic properties of bulk matter, *i.e.* uniform matter of sufficient spatial extension to render finite-size effects (including those from any surfaces) insignificant. In the micro-canonical representation, the state of the system is given in terms of the basic mechanical densities, the (baryon) charge density ρ and the energy density ε which we take as a thermal energy, $\kappa = \frac{1}{2}d\rho T$, plus a compressional energy, $w_0(\rho)$, where d is an adjustable parameter (equal to three for an ordinary gas). Further adjustable parameters appear in the compressional energy density, $w_0(\rho)$, which is specified in App. A.

The key thermodynamic quantity is the entropy density $\sigma(\varepsilon, \rho)$, which we express in terms of the entropy density $\delta(\kappa, \rho)$ for a generalized ideal classical gas of density ρ and thermal density κ ,

$$\sigma(\varepsilon, \rho) \equiv \delta(\varepsilon - w_0(\rho), \rho) = \frac{5}{6}d\rho - \frac{1}{3}d\rho \ln \frac{\rho}{\rho_T}, \quad (1)$$

where we have defined the thermal density as

$$\rho_T(\varepsilon, \rho) \equiv \left[\frac{2\pi m}{h^2} T(\varepsilon, \rho) \right]^{3/2}, \quad (2)$$

with $T(\varepsilon, \rho) = \frac{2}{d}[\varepsilon - w_0(\rho)]/\rho$ (see below). The Lagrange coefficients $\beta = 1/T$ and $\alpha = -\mu/T$ are given by

$$\beta(\varepsilon, \rho) \equiv \partial_\varepsilon \sigma(\varepsilon, \rho) = \partial_\kappa \delta(\kappa - w_0(\rho), \rho) = \delta_\kappa, \quad (3)$$

$$\alpha(\varepsilon, \rho) \equiv \partial_\rho \sigma(\varepsilon, \rho) = \partial_\rho \delta(\kappa - w_0(\rho), \rho) = \delta_\rho - \delta_\kappa w'_0, \quad (4)$$

with $\delta_\kappa \equiv \partial_\kappa \delta(\kappa, \rho)$, $\delta_\rho \equiv \partial_\rho \delta(\kappa, \rho)$, and $w'_0 \equiv \partial_\rho w_0(\rho)$. Thus, the temperature and the chemical potential are

$$T(\varepsilon, \rho) = \frac{1}{\beta} = \frac{2}{d} \frac{\varepsilon - w_0(\rho)}{\rho} = \frac{2}{d} \frac{\kappa}{\rho}, \quad (5)$$

$$\mu(\varepsilon, \rho) = -\alpha T = \frac{1}{3}dT \ln \frac{\rho}{\rho_T} + w'_0(\rho). \quad (6)$$

The pressure and the enthalpy density may be obtained subsequently,

$$p(\varepsilon, \rho) = \sigma T - \varepsilon + \mu \rho = \frac{1}{3}d\rho T - w_0 + \rho w'_0, \quad (7)$$

$$h(\varepsilon, \rho) \equiv p + \varepsilon = \frac{5}{6}d\rho T + \rho w'_0. \quad (8)$$

Two bulk systems with the densities (ε_1, ρ_1) and (ε_2, ρ_2) are in mutual thermodynamic equilibrium iff the total entropy is stationary under arbitrary exchanges of energy and charge, yielding the requirement that they have equal temperatures, chemical potentials, and pressures: $\beta_1 \doteq \beta_2 \equiv \beta_0$, $\alpha_1 \doteq \alpha_2 \equiv \alpha_0$, $p_1 \doteq p_2 \equiv p_0$. Thus phase coexistence requires that the gradient of $\sigma(\varepsilon, \rho)$, $(\sigma_\varepsilon, \sigma_\rho) \equiv (\partial_\varepsilon \sigma, \partial_\rho \sigma)$, be the same at the two phase points and, furthermore (since $p = T[\sigma - \beta\varepsilon - \alpha\rho]$), that the tangent to $\sigma(\varepsilon, \rho)$ at these two points be common. Furthermore, local thermodynamic stability requires that the

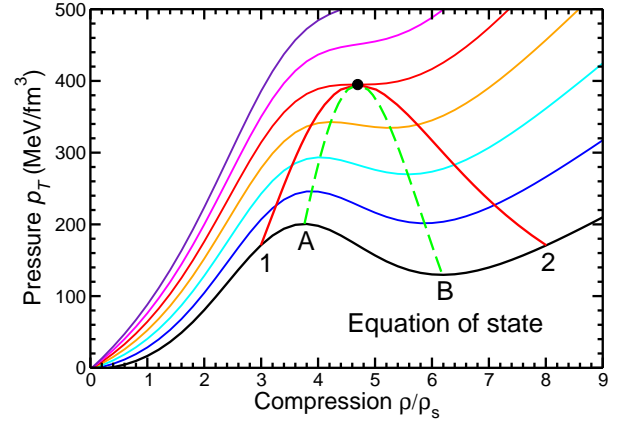


FIG. 1: The equation of state $p_T(\rho)$: The pressure p as a function of the density ρ for a range of temperatures, $T/T_c = 0, \frac{1}{4}, \frac{1}{2}, \frac{3}{4}, 1, \frac{5}{4}, \frac{3}{2}$, obtained with the adopted model. The phase coexistence (solid) and the spinodal (dashes) boundaries are indicated; they coincide at the critical point (dot).

second variation of the entropy be positive under such exchanges, yielding the requirement that the curvature matrix of $\sigma(\varepsilon, \rho)$ be positive definite. Consequently, the region of spinodal instability is delineated by the occurrence of a vanishing curvature eigenvalue.

In the canonical representation ε is replaced by T , and the free energy density is then of special interest,

$$\begin{aligned} f_T(\rho) &\equiv \varepsilon_T(\rho) - T\sigma_T(\rho) = \mu_T(\rho)\rho - p_T(\rho) \\ &= \rho T \ln \frac{\rho}{\rho_T} - \rho T + w_0(\rho), \end{aligned} \quad (9)$$

where the subscript T indicates that the quantity is obtained at the specified temperature. We also note that the slope of the free energy density is the chemical potential, $\partial_\rho f_T(\rho) = \mu_T(\rho)$.

For $w_0(\rho)$ we use an interpolated form that produces a first-order phase transition (see App. A). To achieve a semi-quantitative correspondence with expectations for actual baryon-rich matter, we adjust the parameters such that the coexistence densities at $T = 0$ are $\rho_1 = 3\rho_0$ and $\rho_2 = 8\rho_0$, where $\rho_0 \approx 0.153 \text{ fm}^{-3}$ is the nuclear saturation density; the associated zero-temperature specific heat is then $w_0(\rho_2) - w_0(\rho_1) = 590 \text{ MeV/fm}^3$. Furthermore, the value $d = 5.5$ yields a critical temperature of $T_c = 170 \text{ MeV}$; the critical density is then $\rho_c = 4.70\rho_0$. Other values of particular interest are listed in Table I. (These values are of course somewhat arbitrary but will serve well for illustrative purposes.) The resulting equation of state, $p_T(\rho)$, is shown in Fig. 1, while Fig. 2 displays the associated phase diagram expressed in terms of the mechanical densities ρ and ε . The more familiar (ρ, T) phase diagram, for which the energy density ε has been replaced by the temperature T , is shown in Fig. 3. It is important to recognize that whereas the transformation from ε to T is always unique, the reverse transformation is triple-valued in the presence of a phase transition: Any (ρ, T) phase point inside the phase coex-

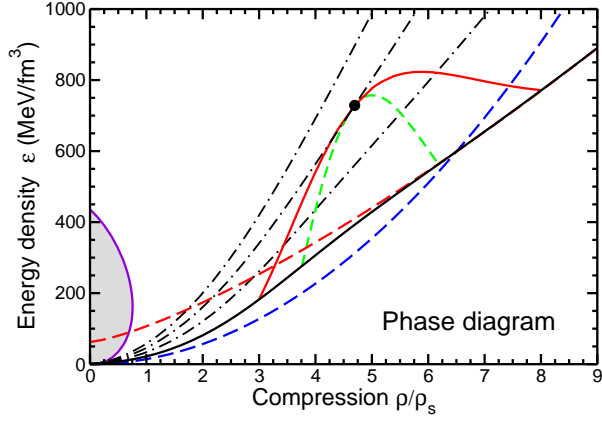


FIG. 2: The phase diagram in the ρ - ε plane, as obtained from the equation of state (Fig. 1), with the phase coexistence boundary (solid, red), the (isothermal) spinodal boundary (short dashes, green), and the critical point (dot) indicated. The hadronic freezeout line (lower left) is included for reference (from Ref. [15]). Also shown are the two functions $w_H(\rho)$ (dashed blue curve) and $w_Q(\rho)$ (dashed red curve) between which the compressional energy $w_0(\rho)$ (solid curve) is interpolated, as well as three isentropic phase trajectories (dot-dashed curves), for which $\rho\delta\varepsilon = (\varepsilon + p)\delta\rho$.

istence region in Fig. 3 could arise any of three different (ρ, ε) phase points in Fig. 2.

At a given temperature T , bulk matter at the two different densities ρ_1 and ρ_2 are in mutual thermodynamic equilibrium if the corresponding tangents of $f_T(\rho)$ are common: the two chemical potentials are then equal since $\mu_T(\rho) = \partial_\rho f_T(\rho)$, and the relation $p_T(\rho) = \mu_T(\rho)\rho - f_T(\rho)$ guarantees that also the two pressures match. Thus phase coexistence at $T = 0$ requires that the tangents of $w_0(\rho)$ at the two densities be common. [We have used this property to guide our choice of mean field.] As the temperature is increased, the difference between the two coexistence densities will steadily shrink until they coincide at the critical temperature T_c .

At supercritical temperatures ($T > T_c$) the pressure increases steadily with T , $\partial_\rho p_T > 0$, whereas its behavior is undulatory at subcritical temperatures: when the density is increased from the lower to the higher coexistence density, the pressure exhibits first a maximum and then a minimum. The associated densities ρ_A and ρ_B where $p_T(\rho)$ is stationary delineate the region of mechanical instability, within which $\partial_\rho p_T(\rho)$ is negative. Since $\partial_\rho p_T(\rho) = \frac{d}{3}T + \rho w_0''(\rho)$, the spinodal boundary densities at $T = 0$ are determined by $\rho w_0''(\rho) \doteq 0$ and $w_0''(\rho)$ is negative in between. The region of mechanical instability shrinks steadily as T is increased and disappears at T_c , which is thus determined by the condition $\frac{d}{3}T_c + \rho_m w_0''(\rho_m) \doteq 0$, where ρ_m is the density at which $\rho w_0''(\rho)$ is most negative. The adopted compressional energy density $w_0(\rho)$ is depicted in Fig. 1 together with the coexistence and spinodal boundaries.

Dynamical transport calculations suggest that the ex-

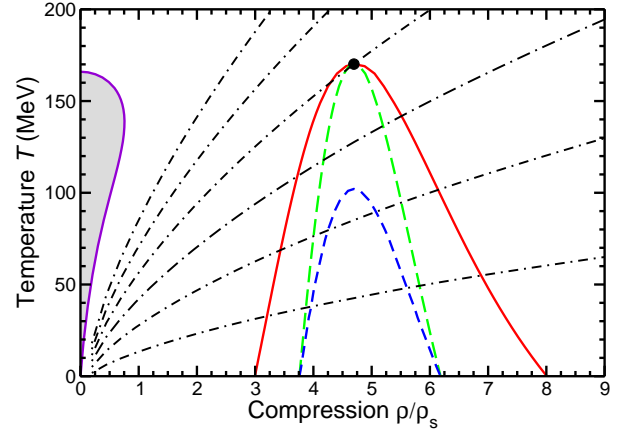


FIG. 3: The phase diagram in the ρ - T plane indicating the phase coexistence boundary (solid), the isothermal spinodal boundary (long dashes), the isentropic spinodal boundary (short dashes), and the critical point (dot). Also shown are several isentropic phase trajectories, for which $\rho\delta\varepsilon = (\varepsilon + p)\delta\rho$.

pansion stage in a nucleus-nucleus collision proceeds in an approximately isentropic manner [16], *i.e.* the entropy per (net) baryon remains nearly constant. Since $T\rho^2\delta(\sigma/\rho) = (\rho\delta\varepsilon - \mu\rho\delta\rho) - (h\delta\rho - \mu\rho\delta\rho) = \rho\delta\varepsilon - h\delta\rho$, the isentropic trajectories in the (ρ, ε) phase plane are characterized by $\rho\delta\varepsilon \doteq h\delta\rho$. Figs. 2 and 3 display several such isentropic phase trajectories and they are seen to not be noticeably affected by the presence of the phase transition. This feature brings out the fact that the locations of the boundaries for thermodynamic and mechanical instability, including the critical point itself, result from a rather subtle interplay between the underlying interactions. One may therefore expect that the overall phase evolution obtained in a dynamical transport calculation is not very sensitive to the specific phase structure.

III. GRADIENT CORRECTIONS

The above thermodynamics discussion applies to bulk matter, *i.e.* large and uniform systems. In heavy-ion physics, the systems encountered are neither and it is therefore practically important to extend the treatment to systems whose densities vary with the location, $\tilde{\varepsilon}(\mathbf{r})$ and $\tilde{\rho}(\mathbf{r})$, where we use a tilde over a quantity as a reminder that it pertains to a non-uniform system.

As a simple way to take approximate account of finite range effects, we employ a gradient correction in the compressional energy. (A gradient term was also employed in recent hydrodynamical studies of the hadron-quark first-order phase transition [17].) Accordingly, we write the local interaction-energy density on the form

$$\begin{aligned} \tilde{w}(\mathbf{r}) &= w_0(\tilde{\rho}(\mathbf{r})) + \frac{1}{2}C(\nabla\tilde{\rho}(\mathbf{r}))^2 \\ &= w_0(\tilde{\rho}(\mathbf{r})) + \frac{1}{2}a^2\varepsilon_g\left(\frac{\nabla\tilde{\rho}(\mathbf{r})}{\rho_g}\right)^2. \end{aligned} \quad (10)$$

It is convenient to write the strength of the gradient term on the form $C = a^2 \varepsilon_g / \rho_g^2$, where ρ_g is a characteristic charge density and ε_g is a characteristic energy density. Since we are here particularly interested in the dynamics in the phase transition region, we choose the phase point (ρ_g, ε_g) to be in the middle of the phase coexistence region, $\rho_g \doteq \rho_c = 4.70 \rho_0$ and $\varepsilon_g \doteq \varepsilon_{T=T_c/2}(\rho_c) = \frac{1}{2}(w_0(\rho_c) + \varepsilon_c) = 561 \text{ MeV/fm}^3$. The strength of the gradient term is then governed by the length a which we consider to be somewhat adjustable. Our present calculations have been made with $a = 0.2 \text{ fm}$.

The introduction of the gradient term leads to gradient corrections in the expressions for the various thermodynamic quantities. In order to derive those, we start from the entropy density, which we assume to still have the form $\tilde{\sigma}(\mathbf{r}) = \tilde{\sigma}(\tilde{\kappa}(\mathbf{r}), \tilde{\rho}(\mathbf{r})) = \tilde{\sigma}(\tilde{\varepsilon}(\mathbf{r}) - \tilde{w}(\mathbf{r}), \tilde{\rho}(\mathbf{r}))$, where $\tilde{\kappa}(\mathbf{r}) = \tilde{\varepsilon}(\mathbf{r}) - \tilde{w}(\mathbf{r})$ is the local thermal energy density. A variation of the total entropy $S[\tilde{\varepsilon}(\mathbf{r}), \tilde{\rho}(\mathbf{r})] = \int d\mathbf{r} \tilde{\sigma}(\mathbf{r})$ then yields the local Lagrange coefficients $\tilde{\beta}$ and $\tilde{\alpha}$,

$$\tilde{\beta}(\mathbf{r}) \doteq \frac{\delta S}{\delta \tilde{\varepsilon}(\mathbf{r})} = \partial_{\tilde{\kappa}}(\tilde{\kappa}(\mathbf{r}), \tilde{\rho}(\mathbf{r})) = 1/\tilde{T}(\mathbf{r}), \quad (11)$$

$$\begin{aligned} \tilde{\alpha}(\mathbf{r}) \doteq \frac{\delta S}{\delta \tilde{\rho}(\mathbf{r})} &= \partial_{\tilde{\rho}}(\tilde{\kappa}(\mathbf{r}), \tilde{\rho}(\mathbf{r})) - \tilde{\beta}(\mathbf{r}) w'_0(\tilde{\rho}(\mathbf{r})) \\ &+ C \nabla(\tilde{\beta}(\mathbf{r}) \cdot \nabla \tilde{\rho}(\mathbf{r})) = -\tilde{\mu}(\mathbf{r})/\tilde{T}(\mathbf{r}). \end{aligned} \quad (12)$$

Using that the entropy density gradient is then given by

$$\nabla \tilde{\sigma}(\mathbf{r}) = \tilde{\beta}(\mathbf{r}) \nabla \tilde{\varepsilon}(\mathbf{r}) + \tilde{\alpha}(\mathbf{r}) \nabla \tilde{\rho}(\mathbf{r}) - C \nabla(\tilde{\beta}(\mathbf{r}) (\nabla \tilde{\rho}(\mathbf{r}))^2), \quad (13)$$

we see that the following expression for the local pressure,

$$\tilde{p}(\mathbf{r}) = \tilde{\sigma}(\mathbf{r}) \tilde{T}(\mathbf{r}) - \tilde{\varepsilon}(\mathbf{r}) + \tilde{\mu}(\mathbf{r}) \tilde{\rho}(\mathbf{r}) + C(\nabla \tilde{\rho}(\mathbf{r}))^2, \quad (14)$$

leads to the relation

$$\nabla \frac{\tilde{p}(\mathbf{r})}{\tilde{T}(\mathbf{r})} = -\tilde{\varepsilon}(\mathbf{r}) \nabla \tilde{\beta}(\mathbf{r}) - \tilde{\rho}(\mathbf{r}) \nabla \tilde{\alpha}(\mathbf{r}), \quad (15)$$

which can be regarded as a generalization of the familiar thermodynamic relation $\delta(p/T) = -\varepsilon \delta\beta - \rho \delta\alpha$. This relation ensures that $\tilde{p}(\mathbf{r})$ will be constant whenever $\tilde{T}(\mathbf{r})$ and $\tilde{\mu}(\mathbf{r})$ are. We also note that the gradient correction to the compressional energy migrates directly into the free energy density,

$$\begin{aligned} \tilde{f}_T(\mathbf{r}) &= \kappa_T(\tilde{\rho}(\mathbf{r})) + \tilde{w}(\mathbf{r}) - T \partial(\kappa_T(\tilde{\rho}(\mathbf{r})), \tilde{\rho}(\mathbf{r})), \\ &= f_T(\tilde{\rho}(\mathbf{r})) + \frac{1}{2} C (\nabla \tilde{\rho}(\mathbf{r}))^2. \end{aligned} \quad (16)$$

IV. INTERFACE EQUILIBRIUM

Once the finite-range effects have been included in the thermodynamics, one may treat the interface between two coexisting phases. For this purpose, we consider a semi-infinite geometry with the two coexisting systems having a planar interface perpendicular to the x direction. The coexistence values of temperature, chemical potential, and pressure are denoted by T_0 , μ_0 , and p_0 .

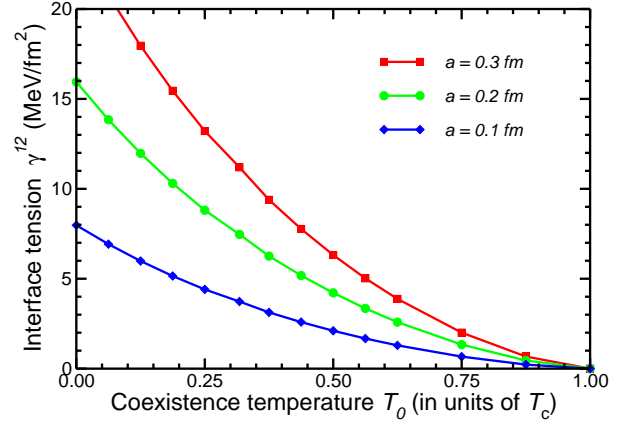


FIG. 4: The specific interface tension $\gamma^{12}_{T_0}$ as a function of the coexistence temperature T_0 for various values of the range a .

We first note that global equilibrium, including equilibrium between two bulk systems with a common interface, requires that the total entropy S be constant under variations $\delta \tilde{\varepsilon}(x)$ and $\delta \tilde{\rho}(x)$ that conserve the total energy $E = \int dx \tilde{\varepsilon}(x)$ and the total (net) charge $B = \int dx \tilde{\rho}(x)$,

$$\begin{aligned} 0 &\doteq \delta S - \beta_0 \delta E - \alpha_0 \delta B \\ &= \delta \int dx [\tilde{\sigma}(x) - \beta_0 \tilde{\varepsilon}(x) - \alpha_0 \tilde{\rho}(x)] \\ &= \int dx \left\{ [\tilde{\beta}(x) - \beta_0] \delta \tilde{\varepsilon}(x) + [\tilde{\alpha}(x) - \alpha_0] \delta \tilde{\rho}(x) \right\}, \end{aligned} \quad (17)$$

thus implying spatial constancy of the temperature and the chemical potential, $\tilde{\beta}(x) \doteq \beta_0$ and $\tilde{\alpha}(x) \doteq \alpha_0$, as one should expect.

Therefore, assuming that the temperature is constant, $\tilde{\beta}(x) = \beta_0 = 1/T_0$, it is convenient to work in the canonical framework and our analysis is then similar to that carried out by Ravenhall *et al.* [18]. With the temperature given, the local density $\tilde{\rho}(x)$ determines the local energy density, $\tilde{\varepsilon}(x) = \frac{d}{2} \tilde{\rho}(x) T_0 + \tilde{w}(x)$, and the local entropy density is then in turn determined, $\tilde{\sigma}(x) = \partial(\tilde{\varepsilon}(x) - \tilde{w}(x), \tilde{\rho}(x)) = \partial(\frac{d}{2} \tilde{\rho}(x) T_0, \tilde{\rho}(x))$. The local free energy density is then readily obtained,

$$\tilde{f}(x) = \tilde{\varepsilon}(x) - T_0 \tilde{\sigma}(x) = f_{T_0}(\tilde{\rho}(x)) + \frac{1}{2} C (\partial_x \tilde{\rho}(x))^2, \quad (18)$$

where $f_T(\rho)$ is the free energy density in bulk matter at temperature T and density ρ (see Sect. II). The corresponding bulk chemical potential is $\mu_T(\rho) = \partial_{\rho} f_T(\rho)$, while the bulk pressure is $p_T(\rho) = \mu_T(\rho) \rho - f_T(\rho)$.

The condition for equilibrium can now be expressed as

$$\begin{aligned} 0 &\doteq \delta \int dx [\tilde{f}(x) - \mu_0 \tilde{\rho}(x)] \\ &= \int dx [\mu_{T_0}(\tilde{\rho}(x)) - C \partial_x^2 \tilde{\rho}(x) - \mu_0] \delta \tilde{\rho}(x), \end{aligned} \quad (19)$$

which then requires

$$C \partial_x^2 \tilde{\rho}(x) \doteq \mu_{T_0}(\tilde{\rho}(x)) - \mu_0 = \partial_{\rho} \Delta f(\tilde{\rho}(x)). \quad (20)$$

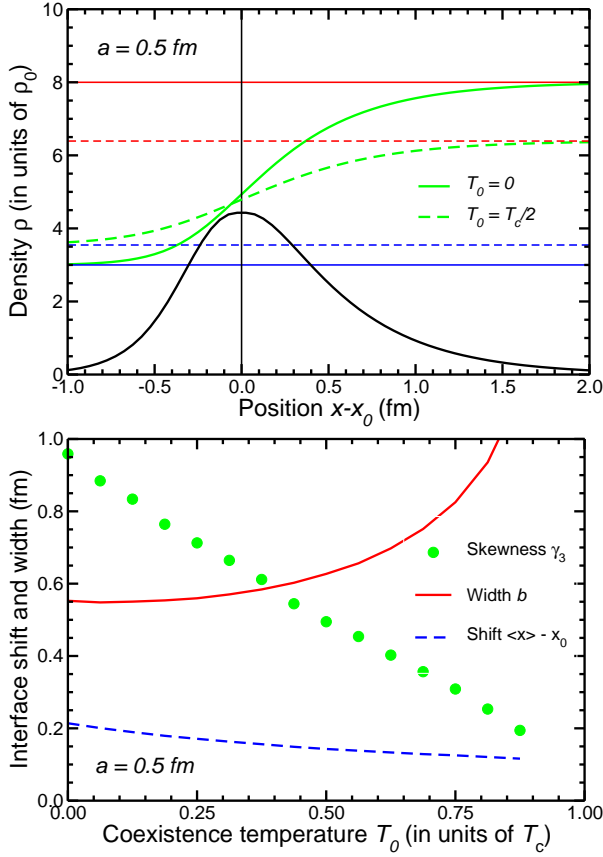


FIG. 5: *Top*: The surface profile $\tilde{\rho}(x)$ for $T = 0$ (solid) and $T = \frac{1}{2}T_c$ (dashed), using as a reference for x the position x_0 where the chemical potential equals the coexistence value of the bulk chemical potential, $\mu_T(\tilde{\rho}(x = x_0)) \doteq \mu_0(T)$. The limiting (coexistence) densities are shown by the horizontal lines, while the bottom curve is the interface location function $g(x)$ for $T = 0$. *Bottom*: The mean location \bar{x} of the interface and its width b as functions of temperature. Also shown is the profile skewness parameter $\gamma_3 \equiv \langle (x - \bar{x})^3 \rangle / b^3$.

Here $\Delta f(\rho)$ is the difference between the free energy density of a uniform system of density ρ , $f_{T_0}(\rho)$, and the corresponding “Maxwell” free energy density, defined as the free energy density along the common tangent,

$$f_{T_0}^M(\rho) \equiv f_{T_0}(\rho_i) + \mu_0(\rho - \rho_i) \leq f_{T_0}(\rho), \quad (21)$$

where ρ_i refers to either one of the two coexistence densities. Thus $\Delta f(\rho)$ can be thought of as the free energy (density) gained by performing a phase mixture.

The equilibrium condition (20) for the density profile $\tilde{\rho}(x)$ is formally equivalent to an equation of motion for a particle of mass C moving in the potential $V(\rho) = -\Delta f(\rho)$, with ρ denoting the coordinate and x the time. (We note that $\Delta f(\rho)$ vanishes at the two coexistence densities and is positive in between.) Conservation of the corresponding energy $\frac{1}{2}C(\partial_x \tilde{\rho})^2 + V$ (which

vanishes) then determines the gradient at each position,

$$\partial_x \tilde{\rho}(x) = \left[\frac{2}{C} \Delta f(\tilde{\rho}(x)) \right]^{\frac{1}{2}}. \quad (22)$$

The local excess in the free energy density due to the interface (see App. C) is given by

$$\begin{aligned} \tilde{f}_{T_0}^{12}(x) &= \tilde{f}(x) - f_{T_0}^M(\tilde{\rho}(x)) \\ &= \Delta f(\tilde{\rho}(x)) + \frac{1}{2}C(\partial_x \tilde{\rho}(x))^2 = 2\Delta f(\tilde{\rho}(x)). \end{aligned} \quad (23)$$

The total deficit in free energy per unit interface area, equal to the interface tension, is then given by [23]

$$\begin{aligned} \gamma_{T_0}^{12} &= \int_{-\infty}^{+\infty} dx \tilde{f}_{T_0}^{12}(x) = 2 \int \frac{d\tilde{\rho}(x)}{dx} \Delta f(\tilde{\rho}(x)) \\ &= \int_{\rho_1}^{\rho_2} d\rho [2C\Delta f(\rho)]^{\frac{1}{2}} = a \int_{\rho_1}^{\rho_2} \frac{d\rho}{\rho_g} [2\varepsilon_g \Delta f(\rho)]^{\frac{1}{2}}. \end{aligned} \quad (24)$$

We note that this quantity can be obtained without explicit knowledge of the interface density profile $\tilde{\rho}(x)$ and it scales directly with the length parameter a . It is shown in Fig. 4 as a function of temperature. As expected, it decreases steadily from its maximum value at $T = 0$ until it vanishes at T_c . With the (somewhat arbitrary) parameter values adopted, the zero-temperature interface tension is $\gamma_0^{12} \approx 16 \text{ MeV/fm}^3$, about 16 times the familiar nuclear surface tension. This value lies near the lower end of the rather wide range of expected values for the tension between quark and nuclear matter (typical low values are 10–20 MeV/fm², while typical high values are 50–100 MeV/fm², see for example Refs. [19, 20]).

The density profile itself, $\tilde{\rho}(x)$, can be obtained by integrating Eq. (22),

$$\tilde{\rho}(x) = \tilde{\rho}(x_0) + \rho_c \int_{x_0}^x \left[\frac{2}{\varepsilon_g} \Delta f(\tilde{\rho}(x)) \right]^{\frac{1}{2}} \frac{dx}{a}, \quad (25)$$

where x_0 is some location where the density is known. We note that it would not be feasible to start the integration at $x_0 \rightarrow \pm\infty$, where $\tilde{\rho}(x_0) \rightarrow \rho_i$, since the gradient vanishes in the same limit, $\tilde{\rho}_x(x_0) \rightarrow 0$. Instead, we take x_0 to be that location where the function $\Delta f(\tilde{\rho}(x))$ has its maximum. Since the derivative $\partial_\rho \Delta f(\rho) = \mu_{T_0}(\rho) - \mu_0$ thus vanishes at $\rho = \tilde{\rho}(x_0)$, it follows that the local bulk chemical potential at x_0 matches the coexistence value, $\mu_{T_0}(\tilde{\rho}(x_0)) = \mu_0$, and this relation can be used to find the starting density value $\tilde{\rho}(x_0)$. [The local bulk chemical potential $\mu_{T_0}(\rho)$ must match the coexistence value $\mu_0 = \mu_{T_0}(\rho_i)$ for some intermediate density because $\mu_{T_0}(\rho)$ exhibits an undulation between ρ_1 and ρ_2 , going first through a maximum $\mu_{T_0}(\rho_A) > \mu_0$ and then through a minimum $\mu_{T_0}(\rho_B) < \mu_0$, so it must equal μ_0 somewhere between ρ_A and ρ_B .]

The density profile $\tilde{\rho}(x)$ is shown in Fig. 5 for $T_0 = 0$ and $T_0 = \frac{1}{2}T_c$. At each temperature, it scales horizontally with the length parameter a . The interface profile can be characterized by the cumulants of the associated

interface location function, $g(x) = \tilde{\rho}_x(x)/(\rho_2 - \rho_1)$ (see App. C). So the mean interface location is $\bar{x} = \langle x \rangle \equiv \int dx x g(x)$, while its width b is the corresponding dispersion, $b^2 = \langle (x - \bar{x})^2 \rangle$. A convenient measure of the profile skewness is given by the dimensionless parameter $\gamma_3 \equiv \langle (x - \bar{x})^3 \rangle / b^3$. As the temperature is increased, the profile grows progressively wider and more symmetric, while its mean location moves closer to x_0 . With the adopted parameter values we find $\bar{x} - x_0 = 1.01 a$, $b = 2.62 a$, and $\gamma_3 = 0.96$ at $T_0 = 0$.

It should be noted that in the present simple treatment, where the finite range is taken into account by means of a gradient term, the interface tension as well as the detailed density profile shape reflect the specific density dependence of the free energy $f_T(\rho)$, *i.e.* they follow directly from the employed bulk equation of state, apart from scalings related to the strength of the gradient term.

V. COLLECTIVE MODES

We now wish to study the dynamical response to the introduction of small density undulations imposed on a system that is static and uniform, $\delta\varepsilon(\mathbf{r}) = \tilde{\varepsilon}(\mathbf{r}) - \bar{\varepsilon}$ and $\delta\rho(\mathbf{r}) = \tilde{\rho}(\mathbf{r}) - \bar{\rho}$. We first note that the local change in the pressure is then of a similar form, $\delta p(\mathbf{r}) = \tilde{p}(\mathbf{r}) - \bar{p}$ with $\bar{p} = p(\bar{\varepsilon}, \bar{\rho})$. For simplicity, we assume that the time evolution is described by fluid dynamics and we first disregard dissipation. The equations of motion then arise from energy-momentum conservation, $\partial_\mu T^{\mu\nu} = 0$, together with conservation of (baryon) charge, $\partial_\mu j^\mu = 0$.

Assuming that the local flow velocities $\mathbf{v}(\mathbf{r})$ are non-relativistic, we may ignore v^2 and thus put γ to unity. This yields the following five equations of motion,

$$0 = \partial_\mu T^{\mu 0}(\mathbf{r}, t) \approx \partial_t \delta\varepsilon + \bar{h} \partial_i v^i, \quad (26)$$

$$0 = \partial_\mu T^{\mu i}(\mathbf{r}, t) \approx \bar{h} \partial_t v^i + \partial^i \delta p, \quad (27)$$

$$0 = \partial_\mu j^\mu(\mathbf{r}, t) \approx \partial_t \delta\rho + \bar{\rho} \partial_i v^i, \quad (28)$$

where $\bar{h} = \bar{\varepsilon} + \bar{p}$ is the enthalpy density of the uniform system. As usual, the equations for $T^{\mu\nu}$ can be combined to a sound-wave equation, while a comparison of the first and last equations yields the evolution of the density disturbance in terms of that of the energy disturbance, so

$$\partial_t^2 \delta\varepsilon(\mathbf{r}) = \partial_i \partial^i \delta p(\mathbf{r}), \quad (29)$$

$$\bar{h} \partial_t \delta\rho(\mathbf{r}) = \bar{\rho} \partial_t \delta\varepsilon(\mathbf{r}). \quad (30)$$

It is straightforward to see that, to leading order in the disturbances $\delta\varepsilon(\mathbf{r})$ and $\delta\rho(\mathbf{r})$, the local pressure is

$$\tilde{p}(\mathbf{r}) \approx p(\tilde{\varepsilon}(\mathbf{r}), \tilde{\rho}(\mathbf{r})) - C\bar{\rho}\nabla^2\rho(\mathbf{r}). \quad (31)$$

The first term is the usual local-density approximation, *i.e.* the pressure is calculated as in uniform matter that has been prepared with the local density values, while the second term arises from the gradient correction to the chemical potential (12). Therefore, to the same order,

$$\nabla^2 \delta p(\mathbf{r}) \approx p_\varepsilon \nabla^2 \varepsilon(\mathbf{r}) + p_\rho \nabla^2 \rho(\mathbf{r}) - C\bar{\rho} \nabla^4 \rho(\mathbf{r}), \quad (32)$$

where $p_\varepsilon \equiv \partial_\varepsilon p(\varepsilon, \rho)$ and $p_\rho \equiv \partial_\rho p(\varepsilon, \rho)$ evaluated at the local phase point $(\varepsilon, \rho) = (\tilde{\varepsilon}(\mathbf{r}), \tilde{\rho}(\mathbf{r}))$.

If we require the undulations to be of harmonic form, $\delta\varepsilon(\mathbf{r}) = \varepsilon_{\mathbf{k}} \exp(i\mathbf{k} \cdot \mathbf{r} - i\omega t)$ and $\delta\rho(\mathbf{r}) = \rho_{\mathbf{k}} \exp(i\mathbf{k} \cdot \mathbf{r} - i\omega t)$, then Eq. (30) requires $\bar{h}\rho_{\mathbf{k}} = \bar{\rho}\varepsilon_{\mathbf{k}}$. The dispersion relation is then readily obtained from (29),

$$\omega_{\mathbf{k}}^2 = v_s^2 k^2 + C \frac{\bar{\rho}^2}{\bar{h}} k^4 = v_s^2 k^2 + a^2 \frac{\varepsilon_g}{\bar{h}} \frac{\bar{\rho}^2}{\rho_g^2} k^4. \quad (33)$$

Here the first term is what emerges in ordinary ideal fluid dynamics, with v_s being the isentropic speed of sound (see Eq. (B7)),

$$v_s^2 = p_\varepsilon + \frac{\bar{\rho}}{\bar{h}} p_\rho = -\frac{\bar{T}}{\bar{h}} [\bar{h}^2 \sigma_{\varepsilon\varepsilon} + 2\bar{h}\bar{\rho} \sigma_{\varepsilon\rho} + \bar{\rho}^2 \sigma_{\rho\rho}], \quad (34)$$

with $\sigma_{\varepsilon\rho} \equiv \partial_\varepsilon \partial_\rho \sigma(\varepsilon, \rho)$ evaluated at $(\varepsilon, \rho) = (\bar{\varepsilon}, \bar{\rho})$, *etc.*. This part of the dispersion relation is perfectly linear, $\omega_{\mathbf{k}} = v_s k$. That pathological behavior is modified by the gradient term which generally increases $\omega_{\mathbf{k}}^2$. In the spinodal region, where v_s^2 is negative, the collective frequency is imaginary, $\omega_{\mathbf{k}} = \pm i\gamma_{\mathbf{k}}$, and the gradient term then suppresses the growth of high- k modes. As a result, the growth rate $\gamma_{\mathbf{k}}$ will exhibit a maximum followed by a rapid fall-off to zero as a function of the wave number k , as is familiar from other substances exhibiting spinodal instability [7, 8].

It is instructive to write the growth rate on the form $\gamma_{\mathbf{k}} = |v_s| k (1 - k^2/k_{\max}^2)^{1/2}$ where the maximum wave number for which spinodal instability occurs is given by

$$k_{\max}^2 = \frac{\bar{h} |v_s^2|}{C \bar{\rho}^2} = -\frac{\bar{h}}{\varepsilon_g} \frac{\rho_g^2 |v_s^2|}{\bar{\rho}^2 a^2}. \quad (35)$$

The maximum in $\gamma_{\mathbf{k}}$ occurs at the “optimal” wave number $k_{\text{opt}} = k_{\max}/\sqrt{2}$ and, as the amplification process proceeds, undulations of this size will become dominant and a characteristic spinodal pattern will thus emerge. The corresponding largest growth rate is $\gamma_{\text{opt}} = \frac{1}{2} |v_s| k_{\max} = |v_s| k_{\text{opt}}/\sqrt{2}$. This quantity scales inversely with the length parameter a and the associated optimal wave length $\lambda_{\text{opt}} = 2\pi/k_{\text{opt}}$ thus scales directly with a . Consequently, an increase of a will increase the scale of the most rapidly amplified mode as well as the associated shortest growth time $t_{\text{opt}} = 1/\gamma_{\text{opt}}$.

The spinodal growth rates $\gamma_{\mathbf{k}}$ depend on the environment, as specified for example by $\bar{\rho}$ and \bar{T} . The temperature dependence is illustrated in Fig. 6 for $\bar{\rho} = \rho_c$, while the density dependence is shown in Fig. 7. $\gamma_{\mathbf{k}}(\bar{\rho}, \bar{T})$ generally vanishes along the spinodal boundary and it decreases as a function of temperature. With the present model, we thus find that the fastest mode at $\bar{\rho} = \rho_c$ has a wave length of $\lambda_{\text{opt}} \approx 3 \text{ fm}$ and a growth time of $t_{\text{opt}} \approx 1.0 \text{ fm}/c$. As the temperature is raised, the maximum wave number k_{\max} decreases as do the optimal values k_{opt} and γ_{opt} . While the obtained temperature dependence is quite significant, it should be recognized that the thermal properties of the present model may

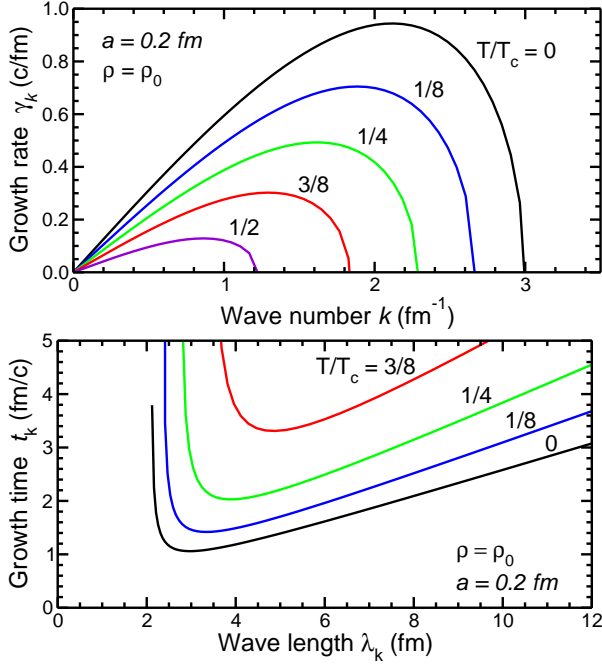


FIG. 6: The growth rate γ_k vs. the wave number k (top) and the corresponding growth times $t_k = \hbar/\gamma_k$ vs. the wave length $\lambda_k = 2\pi/k$ (bottom), for various temperatures T at $\rho = \rho_0$.

not be realistic. (By contrast, the spinodal growth rates in nuclear matter are relatively independent of temperature at the low end because of the fermion nature of the constituents [8].) On the other hand, the dependence of $\gamma_k(\rho, T)$ on density is more moderate in the phase region of most rapid growth (as in dilute nuclear matter [8]).

It is important to appreciate that the phase region of instability for ideal fluid dynamics is bounded by the *isentropic* spinodal (where $v_s = 0$) and it therefore lies inside the region of thermodynamic instability which is bounded by the *isothermal* spinodal (see Fig. 3). There are unstable isentropic modes whenever $v_s^2 < 0$. Insertion of the susceptibilities $\sigma_{\epsilon\epsilon}, \sigma_{\epsilon\pi}, \sigma_{\pi\pi}$ (see App. B) into Eq. (34) yields an explicit expression for the speed of sound,

$$v_s^2 \equiv \frac{\rho}{h} \left(\frac{\partial p}{\partial \rho} \right)_{s \equiv \sigma/\rho} = \frac{\frac{5}{9}dT + \rho w_0''}{\frac{5}{6}dT + w_0'}, \quad (36)$$

so the condition for instability becomes $\frac{5}{9}dT + \rho w_0'' < 0$. At zero temperature this amounts to $\partial_\rho^2 w_0(\rho) < 0$, which occurs exactly within the isothermal spinodal density region, as one would expect since $T = 0 \Leftrightarrow \sigma = 0$. However, as T is increased, the region of isentropic instability shrinks faster than the region of isothermal instability and it disappears entirely at $T_{\text{max}} = \frac{3}{5}T_c$.

The above analysis was based on ideal fluid dynamics which conserves entropy, $\partial_\mu \sigma^\mu = 0$, where $\sigma^\mu = \sigma u^\mu$ is the entropy current density. We wish to conclude this section by briefly discussing the effects of including viscosity into the fluid-dynamic treatment. Within the non-relativistic framework used for the derivation of the dis-

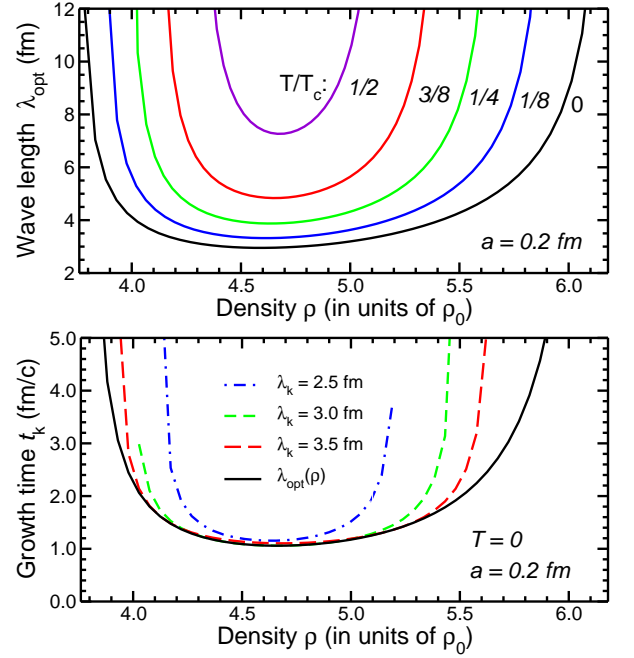


FIG. 7: The optimal wave length λ_{opt} (top) for various temperatures T and the growth time $t_k = \hbar/\gamma_k$ (bottom) at $T = 0$ for several values of the wave length $\lambda_k = 2\pi/k$, as functions of the degree of compression, ρ/ρ_0 .

persion relations for the normal modes in bulk matter, the inclusion of shear and bulk viscosity into the fluid-dynamic treatment changes the pressure gradient by the term $-\nabla[\frac{4}{3}\eta + \zeta]\nabla \cdot \mathbf{v}$ where η and ζ are the shear and bulk viscosity coefficients, respectively. The dispersion equation is then modified accordingly,

$$\omega^2 = v_s^2 k^2 + a^2 \frac{\epsilon_g}{h} \frac{\bar{\rho}^2}{\rho_g^2} k^4 - i[\frac{4}{3}\eta + \zeta] \frac{k^2}{h} \omega, \quad (37)$$

where we have assumed that the combination $\xi \equiv \frac{4}{3}\eta + \zeta$ can be regarded as constant, for simplicity. Clearly, the zero-frequency modes occur for the same wave numbers as before, $k = 0$ and $k = k_{\text{max}}$, and the inclusion of viscosity does not affect the location of the spinodal boundary. (However, if thermal conductivity were included, the spinodal boundary would gradually expand towards the isothermal boundary [18].) To leading order, the viscosity adds a negative imaginary term to the frequency, $-\frac{i}{2}\xi k^2/h$, which in turn gives rise to an exponential damping factor. Furthermore, inside the spinodal region the collective frequencies are still purely imaginary, $\omega = i\gamma_\pm$, and we find

$$\gamma_\pm = \pm \left[|v_s^2| k^2 - a^2 \frac{\epsilon_g}{\bar{\epsilon}} \frac{\bar{\rho}^2}{\rho_g^2} k^4 + \frac{1}{4} \xi^2 \frac{k^4}{h^2} \right]^{\frac{1}{2}} - \frac{1}{2} \xi \frac{k^2}{h}. \quad (38)$$

Thus the growth rate γ_+ is reduced by $\approx \frac{1}{2}\xi k^2/h$ and the optimal wave number becomes smaller as well. Even though the qualitative features will remain the same, the viscous effects may be quantitatively important [17].

In order to illustrate the key role played by the finite range in producing spinodal decomposition, let us briefly consider what would happen without the gradient term. We already noted that the resulting non-viscous dispersion relation would exhibit linear growth, $\gamma_k = |v_s^2|k$, and thus not favor any particular length scale. When viscosity is included, the growth rate would still grow monotonically, $\partial_k \gamma_+(k) > 0$, but level off for large k ,

$$\gamma_+(k \rightarrow \infty) \approx \frac{\bar{\rho}}{\xi} |v_s^2| \left[1 - \frac{3}{4} \frac{\bar{\rho}^2}{\xi^2} \frac{|v_s^2|}{k^2} + \dots \right]. \quad (39)$$

Thus the large- k divergence characteristic of standard ideal fluid dynamics would be eliminated, but there would still not be a preferred length scale.

VI. SPINODAL DECOMPOSITION?

Using the particular model and parameter values chosen here, we now discuss the prospects for spinodal decomposition to occur during a nuclear collision. Although the explored mean-field model is rather simplistic and the specific parameter values are somewhat uncertain, the resulting features appear to be within the range of plausibility. It may therefore be instructive to explore the consequences. Obviously, as further progress is made, both theoretically and experimentally, the models should be appropriately refined.

In order to understand under what experimental conditions spinodal decomposition may actually occur, it is useful to consider how the thermodynamic conditions in the bulk of the collision system evolve in the course of time. Such phase trajectories were studied for gold-gold collisions with a variety of existing dynamical transport models [16] and we shall make use of those results for our estimates. Ref. [16] calculated the evolution of the mechanical phase point $(\rho(t), \varepsilon(t))$ in order to avoid making any assumption about local thermalization; since we are here mainly concerned with the expansion stage, we assume that equilibrium has been established and so we shall frame our discussion in terms of the canonical phase variables $(\rho(t), T(t))$ which are somewhat more intuitive.

Generally speaking, the prospects for spinodal decomposition can be expected to be better the more time the bulk of the matter spends inside the region of spinodal instability. Let us therefore consider how this quantity develops with the collision energy. For the discussion below, we assume that the equation of state has the expected form with a first-order phase transition terminated by a critical point, as drawn schematically in Fig. 8 (see also Fig. 3). It seems natural to introduce a number of threshold values of the collision energy E : E_1 , E_A , E_B , E_2 , E_c . Their meaning is illustrated in Fig. 8 and they will be explained in turn below.

At the lowest collision energies, $E < E_1$, the compressions achieved are insufficient to bring any part of the matter inside the region of phase coexistence. Conse-

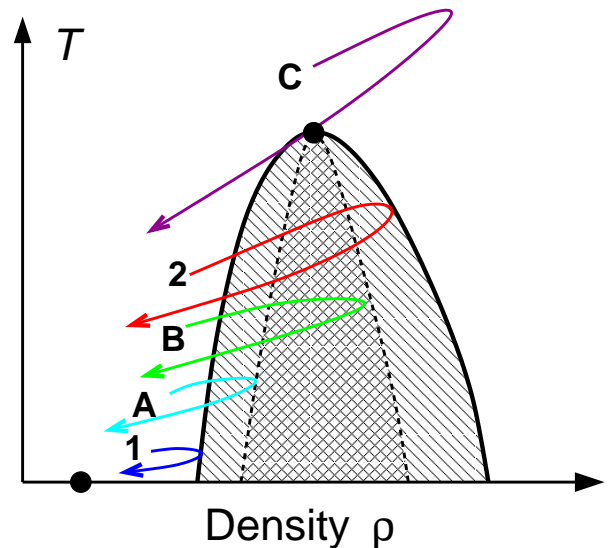


FIG. 8: Illustration of the dynamical phase trajectories for the most compressed matter produced at the various threshold collision energies E_1 , E_A , E_B , E_2 , E_c .

quently, at such low energies, it would probably not be possible to probe the phase transition.

As the collision energy is raised above E_1 , the phase trajectory $(\rho(t), T(t))$ of the most compressed matter makes ever larger incursions into the phase coexistence region. Characterizing such phase trajectories by the highest compression achieved, $\rho_{\max}(E)$, we expect this “turning point” to gradually move across the phase coexistence region as E is raised. It first enters the spinodal region for $E = E_A$ and it has traversed it fully for $E = E_B$, reaching the other side of the coexistence region at $E = E_2$.

At collision energies above E_2 , the steady expansion of the bulk matter subsequent to its maximum compression drags its phase trajectory through the phase coexistence region (and the spinodal region within it). As E is increased the slope of the expansion phase trajectory steepens (see Ref. [16]) and the traversal time becomes steadily shorter, both because the expansion is faster and because the region of instability becomes narrower at the ever higher excitations encountered. At a certain “critical” collision energy, $E = E_c$, the phase trajectory passes right through the critical point (ρ_c, T_c) and at supercritical collision energies, $E > E_c$, the phase trajectory will miss the unstable phase region altogether.

Generally, the evolving local thermodynamic conditions during a collision will differ from one location to another. Consequently, a single collision event gives rise to an entire bundle of phase trajectories and the above discussion pertains to just the phase trajectory of the most compressed matter of the collision system which, for a symmetric collision, is presumably located around the center. Furthermore, there is a dependence on the geometric features of the collision system, such as the nu-

clear sizes and the impact parameter. Thus the precise meaning of the various threshold energies is somewhat fuzzy and they play primarily a conceptual role. This underscores the fact that quantitative predictions must rely on detailed dynamical calculations.

Our special interest here concerns the relatively narrow interval of collision energy within which the turning point lies inside the spinodal region, $E_A < E < E_B$. Intuitively, one would expect that collision energies slightly below E_B would be optimal for maximizing the time spent by the phase trajectory inside the spinodal region. Such collisions, in turn, would presumably be most favorable for the development of spinodal decomposition. The transport calculations reported in Ref. [16] suggest that this optimal beam energy is 5 – 15 GeV per nucleon for a stationary target setup. The precise values depend not only on the specific location of the spinodal phase boundaries, *i.e.* on the specific equation of state (which is still unknown), but also on the complications arising from the non-uniformity of the density and its time evolution.

In order to get a rough idea of the degree of spinodal growth that could be expected during a given collision, we assume that we know the time evolution of the bulk density, $\rho(t)$, and the associated temperature, $T(t)$. As pointed out above, these quantities are local and the present analysis employs suitable average values that can be taken as representative of an extended part of the system. For a given collision energy between E_A and E_B , the phase trajectory $(\rho(t), T(t))$ enters the spinodal region at the time $t = t_i$ and exits it again at the time $t = t_f$. Thus, for $t_i < t < t_f$ the collective dispersion relation yields unstable modes with associated growth rates $\gamma_k(t) \equiv \gamma_k(\rho(t), T(t))$ which serve to amplify irregularities in the density.

An accurate calculation would need to take account not only of the distribution of density fluctuations but also of the fact the entire scenario changes in time (and relatively rapidly). This is beyond our present scope and we seek to obtain a simple estimate by considering the following amplification coefficient [14],

$$\Gamma_0 \equiv \int_{t_i}^{t_f} \gamma_0(t) dt \approx \frac{2}{3} \gamma_{\max} \Delta t, \quad (40)$$

where $\gamma_0(t)$ is the maximum growth rate at the time t , $\gamma_0(t) \equiv \gamma_{\text{opt}}(\rho(t), T(t))$ and γ_{\max} is the largest growth rate overall. The factor of two thirds accounts roughly for the fact that $\gamma_0(t)$ has a parabola-like appearance, starting out from zero at t_i , exhibiting a broad maximum of γ_{\max} , and then dropping to zero again at t_f , so we put $\langle \gamma_0(t) \rangle \approx \frac{2}{3} \gamma_{\max}$. Judging from the transport calculations reported in Ref. [16], we estimate the duration of the spinodal stage to be $\Delta t \equiv t_f - t_i \approx 6 \text{ fm}/c$. To estimate γ_{\max} is more difficult. Our present calculations give an overall fastest growth time of $\approx 1 \text{ fm}/c$, obtained for relatively broad range of densities and for zero temperature. However, the compression achieved in a nuclear collision is inevitably accompanied by a corresponding agitation,

and we therefore expect $T/T_c = \frac{1}{3} - \frac{1}{2}$ to be more realistic. In this connection it should be realized that the rapid decrease of the calculated growth rate as the temperature is increased is to some extent a reflection of the fact that the present instability region is bounded the isentropic rather than the isothermal spinodal line. On the other hand, the inclusion of dissipation (which would expand the region of instability) is expected to slow the dynamics down to a significant degree [17]. Therefore it is probably more realistic to expect the fastest growth time to be several times that most optimistic value, so we use $\gamma_{\max}^{-1} \approx 2 - 4 \text{ fm}/c$

With these rough numbers, we then find the value of the amplification coefficient to be $\Gamma_0 \approx \frac{2}{3} 6 / (2 - 4) = 1 - 2$. The corresponding amplitude growth factor [14] is then given by $G_0 \equiv \exp(\Gamma_0) \approx 2.7 - 7.4$. When trying to judge the significance of this value, one should keep in mind that the density-density correlation function is proportional to the *square* of the amplitude growth factor, *i.e.* $\langle \delta\rho(\mathbf{r}_1) \exp(i\mathbf{r}_{12} \cdot \mathbf{k}) \delta\rho(\mathbf{r}_2) \rangle \sim G_k^2$.

It should also be realized that after the system exits the spinodal instability region of the phase diagram, it has still to traverse the metastable region between the spinodal boundary and the phase coexistence line. While nearly uniform matter is mechanically stable in this regime, this is no longer so for matter having significant deviations from uniformity. Therefore, the undulations resulting from even relatively modest amplifications during the spinodal stage may be further amplified during the metastable stage and thus lead to observationally interesting clumping of the expanding matter.

The above numerical estimates were obtained for the adopted range value of $a = 0.2 \text{ fm}$ which is of course rather uncertain. We recall that it leads to an interface tension of $\gamma_{T=0}^{12} \approx 16 \text{ MeV}/\text{fm}^2$ and an optimal wavelength of $\lambda_{\text{opt}} \approx 4 \text{ fm}$ at $T \approx \frac{1}{3} T_c$. The interface tension is at the lower end of what has been used by various authors [19, 20], but does not appear to be unreasonable considering the large uncertainties on this quantity. As for the wave length, it is of interest to note that a spherical volume having such a diameter would contain a baryon number of $B_0 = \frac{\pi}{6} \lambda_{\text{opt}}^3 \rho_c \approx 24$. At a temperature of half the critical value, the completion of the phase decomposition would distribute this matter approximately evenly between the two coexisting phases, assuming the high-density phase is concentrated in a sphere embedded into the low-density phase. Such a blob of deconfined matter is large enough to constitute a macroscopic statistical source, while at the same time being probably a sufficiently small part of the total system to permit the simultaneous formation of several such blobs and thus make it feasible to perform a size-correlation analysis.

If we were to use only half that range, $a = 0.1 \text{ fm}$, those quantities would decrease correspondingly to $\gamma_{T=0}^{12} \approx 8 \text{ MeV}/\text{fm}^2$, which would be somewhat low in comparison to the existing estimates, though perhaps not impossible, and $\lambda_{\text{opt}}(\frac{1}{3} T_c) \approx 2 \text{ fm}$, leading to $B_0 \approx 3$ which seems too small to constitute a macroscopic source that

could have observational significance. On the other hand, if we were to double the range, $a = 0.4 \text{ fm}/c$, we would obtain $\gamma_{T=0}^{12} \approx 32 \text{ MeV}/\text{fm}^2$, which would seem quite reasonable, but $\lambda_{\text{opt}}(\frac{1}{3}T_c) \approx 8 \text{ fm}$ (hence $B_0 \approx 192$) would be far too large to produce a useful effect.

This analysis reveals that whether a given model leads to spinodal phase decomposition in simulations of nuclear collisions depends rather delicately on the specific values of its parameters. Consequently, it is far from certain that collisions of real nuclei would in fact produce this phenomenon at any collision energy.

The estimates above suggest that collisions within a suitably tuned energy range may produce bulk matter that stays inside the mechanically unstable phase region sufficiently long for some degree of spinodal clumping to occur. However, it is hard to predict whether the amplification of the fluctuations will suffice to bring about the characteristic spinodal enhancement of a certain length scale. Indeed, the degree of amplification might be so marginal that the matter will revert to approximate uniformity after reentering the stable regime and no clumping-like phase separation would then occur.

This uncertainty underscores the need for studying the observable consequences of a spinodal decomposition. Indeed, only if the spinodal phenomenon manifests itself in detectable signals can it be turned into a useful tool for probing the equation of state. It is as of yet far from clear whether any proposed “signals” of the phase decomposition would in fact survive the subsequent expansion stage dominated by hadronic resonances. While current microscopic transport models present useful tools for such investigations, the insight that can be gained will likely remain somewhat limited until we achieve a better understanding of the phase transition dynamics itself.

VII. CONCLUDING REMARKS

The present study was motivated by the need for developing theoretical models that can address the dynamics of the confinement phase transition that is expected to occur during the expansion stage of collisions between heavy nuclei at suitably tuned energies. As a step towards this goal, we have developed a simple model within which we have studied both the collective dispersion relation for the mechanically unstable modes of bulk matter in the spinodal region of the thermodynamic phase diagram *and* the properties of the interface between the two coexisting phases into which such an unstable system seeks to decompose. These properties are central to the phase transition dynamics and since they are fundamentally related it is important they be treated consistently. As far as we are aware, this is the first time that these different properties have been addressed within the same model framework.

The key element is the inclusion of a finite interaction range without which there would be neither an interface tension nor spinodal decomposition. Indeed, a zero-

range model would render any interface perfectly sharp and there would be no associated energy cost, hence no basis for determining the geometric structure of a system composed of coexisting phases (a zero-range model would admit even fractal intermingling of the phases). Furthermore, without a finite range to suppress the dynamics of short wavelength disturbances, the growth rate would increase steadily with wave number (even in the presence of viscosity), hence not display a maximum as is characteristic of spinodal decomposition. Thus, any model that aspires to be of use for phase transition dynamics must incorporate a finite range.

A recent study by Skokov and Voskresensky has sought to accomplish that by means of a gradient term in the free energy functional [17]. In the present study, we take a similar approach by constructing an equation of state in which the interaction-energy density in non-uniform matter contains a gradient term. This can be thought of as approximating a convolution with a kernel of finite range, as is often done for the mean field in low-energy nuclear physics.

Considering that no quantitatively reliable calculations are yet available, we have had to fix the parameters of the equation of state for bulk matter on the basis of our best guess for the location of the coexistence region, including the critical point. Consequently, our results should not be considered as more than suggestive. The additional range parameter entering into the gradient term has been adjusted to yield reasonable values for the interface tension and the spinodal growth rates. Importantly, a change in this range by a factor of two or more would render the model results either implausible (relative to existing estimates) or phenomenologically uninteresting (in that the resulting model would not produce spinodal decomposition in a collision scenario).

With the gradient term included, we have then studied the equilibrium interface between two coexisting phases and determined the temperature dependence of the density profile and the associated interface tension.

In order to address the collective modes in bulk matter, a dynamical model is needed and we have adopted fluid dynamics, which can readily be adapted to the finite-range equation of state. The gradient term suppresses the growth of short wavelengths and thus yields a physically reasonable dispersion relation for the spinodal modes.

Taking guidance from existing phase trajectories extracted from various transport simulations [16], we have used the calculated growth rates to estimate the degree of amplification that might occur when the collision energy is adjusted to maximize the exposure to the spinodal instabilities. The resulting amplification amounts to one or two factors of e , which may suffice to trigger a phase separation due to the subsequent further amplification from the intermediate metastable phase region. While this conclusion gives grounds for guarded optimism, it also brings out the fact that a full dynamical simulation is needed for a more detailed assessment.

Acknowledgements

We wish to acknowledge many helpful discussions with P.F. Bedaque, B. Friman, U. Heinz, V. Koch, R. Sharma, W.J. Swiatecki, and D.N. Voskresensky. This work was supported by the Director, Office of Energy Research, Office of High Energy and Nuclear Physics, Nuclear Physics Division of the U.S. Department of Energy under Contract No. DE-AC02-05CH11231.

APPENDIX A: COMPRESSIONAL ENERGY

The key quantity in the employed illustrative equation of state is the energy density associated with the compression of bulk matter at zero temperature, $w_0(\rho) = \varepsilon_{T=0}(\rho)$. We obtain this basic function by interpolating between a “hadron gas” and a “quark-gluon plasma”,

$$w_0(\rho) = \chi(\rho)w_H(\rho) + [1 - \chi(\rho)]w_Q(\rho), \quad (\text{A1})$$

where the interpolation function is taken as

$$\chi(\rho) = [1 + e^{(\rho - \rho_\chi)/\rho_w}]^{-1} \quad (\text{A2})$$

and each phase is taken to display a simple power form,

$$w_H(\rho) = c_H(\rho/\rho_0)^2, \quad w_Q(\rho) = c_Q(\rho/\rho_0)^{4/3} + B, \quad (\text{A3})$$

$\rho_0 \approx 0.153 \text{ fm}^{-3}$ being the nuclear saturation density.

For a wide range of parameter values, the resulting compressional energy density $w_0(\rho)$ exhibits a region of negative curvature, thus ensuring the existence of a first-order phase transition. [We recall that phase coexistence requires equal chemical potentials, $\mu(\rho_1) \doteq \mu(\rho_2)$, hence equal slopes of $w_0(\rho)$ (since $\mu_{T=0} = \partial_\rho w_0$), as well as equal pressures, $p(\rho_1) = p(\rho_2)$, hence a common tangent of $w_0(\rho)$ (since $p_{T=0} = \mu\rho - f = \rho\partial_\rho w_0 - w_0$).] Adopting the specific values $c_H = 92.6$, $c_Q = 288.9$, and $B = 408.3$ (all in MeV/fm^3) together with $\rho_\chi = 3.2535\rho_0$ and $\rho_w = 0.945\rho_0$, we obtain $\rho_1 = 3\rho_0$ and $\rho_2 = 8\rho_0$ for the zero-temperature coexistence densities. (It would be straightforward to obtain other values by readjusting the parameters.)

The resulting compressional energy density $w_0(\rho)$ is shown in Fig. 1 by the solid (black) curve, while the dashed (blue and red) curves are the individual functions $w_H(\rho)$ and $w_Q(\rho)$. It is apparent from the plot that the coexistence features depend delicately on the parameter values. One would therefore expect any model calculation of the phase structure to be endowed with rather large uncertainties, thus reinforcing the need for experimental information.

Table I summarizes the values of the various quantities of interest at the phase and spinodal boundaries:

| # | T (MeV) | ρ/ρ_0 | ε (MeV/fm ³) | p (MeV/fm ³) | μ (MeV) |
|---|-----------|---------------|--------------------------------------|----------------------------|-------------|
| 1 | 0 | 3.00 | 182 | 171 | 769 |
| A | 0 | 3.76 | 276 | 201 | 829 |
| c | 170 | 4.70 | 729 | 395 | 923 |
| B | 0 | 6.18 | 563 | 130 | 732 |
| 2 | 0 | 8.01 | 772 | 171 | 769 |

TABLE I: Values of the temperature T , compression ρ/ρ_0 , energy density ε , pressure p , and chemical potential μ at the two zero-temperature coexistence points (#1 and #2), the two spinodal boundaries at zero temperature (#A and #B), and the critical point (#c) (see Figs. 1 and 2).

APPENDIX B: SUSCEPTIBILITIES

Mechanical stability is determined by the curvature tensor σ of the entropy density, which in the present model has the elements $\sigma_{\varepsilon\varepsilon}$, $\sigma_{\rho\varepsilon} = \sigma_{\varepsilon\rho}$, $\sigma_{\rho\rho}$, where

$$\sigma_{\varepsilon\varepsilon} \equiv \partial_\varepsilon^2 \sigma(\varepsilon, \rho) = -\frac{d}{2} \frac{\rho}{(\varepsilon - w_0)^2} = -\frac{d}{2} \frac{\rho}{\kappa^2} < 0, \quad (\text{B1})$$

$$\sigma_{\rho\varepsilon} \equiv \partial_\rho \partial_\varepsilon \sigma(\varepsilon, \rho) = \sigma_{\varepsilon\rho} = \frac{d}{2} \frac{1}{\kappa} + \frac{d}{2} \frac{\rho w'_0}{\kappa^2}, \quad (\text{B2})$$

$$\sigma_{\rho\rho} \equiv \partial_\rho^2 \sigma(\varepsilon, \rho) = -\frac{5}{6} \frac{d}{\rho} - d \frac{w'_0}{\kappa} - \frac{d}{2} \frac{\rho w''_0}{\kappa} - \frac{d}{2} \frac{\rho w''_0}{\kappa^2}. \quad (\text{B3})$$

with $\kappa(\varepsilon, \rho) \equiv \varepsilon - w_0(\rho) = \frac{1}{2} d \rho T$. We generally have

$$|\sigma| \equiv \sigma_{\varepsilon\varepsilon} \sigma_{\rho\rho} - \sigma_{\varepsilon\rho}^2 = -\frac{\sigma_{\varepsilon\varepsilon}}{\rho T} \partial_\rho p_T(\rho), \quad (\text{B4})$$

which in the present case amounts to

$$|\sigma| = \frac{2}{d} \frac{\frac{1}{3} d T + \rho w''_0}{\rho^2 T^3}. \quad (\text{B5})$$

Since the occurrence of mechanical instability requires that at least one of the eigenvalues of σ be positive, and $|\sigma|$ is the product of the eigenvalues, it follows that mechanical instability occurs at densities for which $w''_0(\rho)$ is negative and then extends up to the temperature $T_{\text{max}}(\rho) = -\frac{3}{d} \rho w''_0(\rho)$. The critical temperature is the largest of those, $T_c = T_{\text{max}}(\rho_c) = \frac{3}{d} \rho_c w''_0(\rho_c)$.

The isothermal sound speed v_T readily follows,

$$v_T^2 = \frac{\rho}{h} \left(\frac{\partial p}{\partial \rho} \right)_T = -\frac{\rho}{h} \rho T \frac{|\sigma|}{\sigma_{\varepsilon\varepsilon}} = \frac{\frac{1}{3} d T + \rho w''_0}{\frac{5}{6} d T + w'_0}, \quad (\text{B6})$$

where $h \equiv p + \varepsilon$ and we have used $(\partial p / \partial \rho)_T = \partial_\rho p_T(\rho)$, while the isentropic sound speed v_s is given by

$$\begin{aligned} v_s^2 &= \frac{\rho}{h} \left(\frac{\partial p}{\partial \rho} \right)_s = \partial_\varepsilon p(\varepsilon, \rho) + \frac{\rho}{h} \partial_\rho p(\varepsilon, \rho) \\ &= -\frac{T}{h} [h^2 \sigma_{\varepsilon\varepsilon} + 2h\rho \sigma_{\varepsilon\rho} + \rho^2 \sigma_{\rho\rho}] = \frac{\frac{5}{9} d T + \rho w''_0}{\frac{5}{6} d T + w'_0}, \end{aligned} \quad (\text{B7})$$

where $s = \sigma/\rho$ is the entropy per particle and we have used that the requirement $\delta s \doteq 0$ implies $\rho \delta \varepsilon \doteq h \delta \rho$. We note that $v_s^2 \geq v_T^2$ for $T \geq 0$.

APPENDIX C: INTERFACE

Consider a planar interface between two semi-infinite systems and let the bulk values of the charge and energy densities in system i be ε_i and ρ_i , respectively, and assume that $\rho_1 \leq \rho_2$. Presumably the local densities $\rho(x)$ and $\varepsilon(x)$ rapidly approach these asymptotic values away from the interface. We may generally define the *interface location function* [21],

$$g_\rho(x) \equiv \frac{\partial_x \rho(x)}{\rho_2 - \rho_1}, \quad \int_{-\infty}^{+\infty} g_\rho(x) dx = 1, \quad (\text{C1})$$

which peaks near the interface and is normalized to unity. Its moments provide quantitative characteristics of the interface profile and we list here the first three [21],

$$\text{Location: } \bar{x} = \langle x \rangle \equiv \int_{-\infty}^{+\infty} x g_\rho(x) dx, \quad (\text{C2})$$

$$\text{Width: } b = [\langle (x - \bar{x})^2 \rangle]^{1/2}, \quad (\text{C3})$$

$$\text{Skewness: } \gamma_3 = \langle (x - \bar{x})^3 \rangle / b^3. \quad (\text{C4})$$

In order to extract the interface tension, we follow the discussion in Ref. [22]. Thus, the difference between the actual diffuse energy density $\varepsilon(x)$ and that associated with the corresponding sharp-surface configuration that would result if there were no gradient term is given by

$$\varepsilon_{12}(x) = \varepsilon(x) - \varepsilon_i - \frac{\varepsilon_2 - \varepsilon_1}{\rho_2 - \rho_1} (\rho(x) - \rho_i), \quad i = 1, 2. \quad (\text{C5})$$

The function $\varepsilon_{12}(x)$ is obviously smooth and, moreover, it tends quickly to zero away from the interface, so it is indeed peaked in the interface region. (It is elementary to see that it does not matter whether one uses $i = 1$ or $i = 2$ in the above expression.) Its integral is then the total energy deficit associated with the diffuse interface, the *interface tension*,

$$\gamma_{12} \doteq \int_{-\infty}^{+\infty} \varepsilon_{12}(x) dx, \quad (\text{C6})$$

which can thus readily be calculated once the profile densities $\rho(x)$ and $\varepsilon(x)$ are known.

-
- [1] Y. Aoki, G. Endrodi, Z. Fodor, S.D. Katz, K.K. Szabo, *Nature* **443**, 675 (2006).
 - [2] F. Karsch, *Prog. Theor. Phys. Suppl.* **168**, 237 (2007).
 - [3] Z. Fodor, S.D. Katz, K.K. Szabo, *Phys. Lett. B* **568**, 73 (2003).
 - [4] Z. Fodor, S.D. Katz, *JHEP* **04**, 050 (2004).
 - [5] R.V. Gavai, S. Gupta, *Phys. Rev. D* **71**, 114014 (2005).
 - [6] Ph. de Forcrand, O. Philipsen, *LAT2008*, 208 (2008).
 - [7] R.A.L. Jones, *Soft Condensed Matter*, Oxford University Press, 2002 [ISBN 0198505892, 9780198505891].
 - [8] Ph. Chomaz, M. Colonna, J. Randrup, *Phys. Reports* **389**, 263 (2004).
 - [9] B. Borderie *et al.*, *Phys. Rev. Lett.* **86**, 3252 (2001).
 - [10] D. Bower, S. Gavin, *Phys. Rev. C* **64**, 051902 (2001).
 - [11] J. Randrup, *Acta Phys. Hung.* **22**, 69 (2005).
 - [12] V. Koch, A. Majumder, J. Randrup, *Phys. Rev. C* **72**, 064903 (2005).
 - [13] C. Sasaki, B. Friman, K. Redlich, *Phys. Rev. Lett.* **99**, 232301 (2007).
 - [14] J. Randrup, *Phys. Rev. Lett.* **92**, 122301 (2004).
 - [15] J. Randrup, J. Cleymans, *Phys. Rev. C* **74**, 047901 (2006).
 - [16] I.C. Arsene *et al.*, *Phys. Rev. C* **75**, 034902 (2007).
 - [17] V.V. Skokov, D.N. Voskresensky, *nucl-th/0811-3868*; *nucl-th/0903-4335*.
 - [18] D.G. Ravenhall, C.J. Pethick, J.M. Lattimer, *Nucl. Phys. A* **407**, 571 (1983).
 - [19] H. Heiselberg, C.J. Pethick, E.F. Staubo, *Phys. Rev. Lett.* **70**, 1355 (1993).
 - [20] D.N. Voskresensky, M. Yasuhira, T. Tatsumi, *Nucl. Phys. A* **723**, 291 (2003).
 - [21] R.W. Hasse, W.D. Myers, *Geometrical Relationships of Macroscopic Nuclear Physics*, Springer-Verlag, 1988 [ISBN 0-540-17510-5, 0-387-17510-5].
 - [22] W.D. Myers, W.J. Swiatecki, C.S. Wang, *Nucl. Phys. A* **436**, 185 (1985).
 - [23] There are two common notations for the interface tension, σ and γ ; since σ might be confused with the entropy density, we use γ , hoping that it will not be confused with the spinodal growth rate.